Liquid Crystals
Publication details, including instructions for authors and subscription information:
http://www.informaworld.com/smpp/title~content=t713926090

Liquid crystal electrohydrodynamics in the presence of a magnetic field: the dynamic scattering transition

H. M. Shehadeh[a]; J. P. McClymer[a]; E. F. Carr[a]
[a] Department of Physics and Astronomy, University of Maine, Orono, Maine 04469-5709, USA,

Online publication date: 06 August 2010

To cite this Article Shehadeh, H. M. , McClymer, J. P. and Carr, E. F.(2000) 'Liquid crystal electrohydrodynamics in the presence of a magnetic field: the dynamic scattering transition', Liquid Crystals, 27: 10, 1305 — 1316
To link to this Article: DOI: 10.1080/026782900423359
URL: http://dx.doi.org/10.1080/026782900423359

LIQUID CRYSTALS, 2000, VOL. 27, NO. 10, 1305–1316

Liquid crystal electrohydrodynamics in the presence of a magnetic field: the dynamic scattering transition

H. M. SHEHADEH, J. P. MCCLYMER* and E. F. CARR

Department of Physics and Astronomy, University of Maine, Orono, Maine 04469-5709, USA

(*Received 4 March 1999; in final form 24 April 2000; accepted 24 April 2000*)

We have studied electrohydrodynamic convection in the nematic liquid crystal MMBA in the conduction regime in the presence of a competing magnetic field. This field substantially alters the behaviour of the system, causing a metastable surface deformation and travelling waves. The magnetic field also alters the transition between the two dynamic scattering modes so that both states retain anisotropic ordering. A scaling relation is found describing this hysteretic transition. We report the existence of a stable mixed state of DSM 1 and DSM 2.

1. Introduction

Liquid crystals flow like liquids yet have weak, non-zero, elastic constants allowing strong response to external fields. One such well studied response is the formation of anomalous alignment and convective flow cells caused by subjecting nematic liquid crystals to low frequency electric fields (Carr–Helfrich effect) [1]. The addition of a magnetic field to this system, parallel or perpendicular to the electric field, has been investigated both theoretically [2] and experimentally [3–6]. It is thus surprising that our experimental investigation of the effects of competing magnetic and electric fields show some new results. Among these results is the observation of a rubust travelling wave state. These waves are robust in the sense that, unlike for other travelling wave states reported in similar systems [7–10], we do not need to use very thin samples or to pick a frequency very near the cut-off frequency. Instead we observe travelling waves for a wide range of sample thickness and over a wide range of frequency. These results have been reported elsewhere [11, 12]. While the travelling waves are not directly the subject of this paper, there is a connection between them and the purpose of this paper, which is to report on the nature of the transition between the two dynamic scattering mode states in the presence of a magnetic field. In order better to place these results in context, we first briefly review the relevant background.

When a nematic liquid crystal with negative dielectric anisotropy, such as MBBA (*N*-(*p*-methoxybenzylidene)-*p*-butylanaline), is subjected to an a.c. electric field perpendicular to the director, it undergoes a series of pattern forming transitions that depend on the driving voltage and frequency [1, 13]. Two frequency regimes exist. In the low frequency conduction regime the ionic impurities follow the changing electric field, setting up a stationary director pattern. The ions set up an internal electric field causing the director to rotate away from the initial orientation. The resulting flow-alignment interaction cause the director to align nearly parallel to the external field at the flow alignment angle. This behaviour is described by the Carr–Helfrich mechanism and subsequent modifications. In the higher frequency dielectric regime the ionic impurities can no longer follow the changing electric field. These two regimes are separated by a well defined 'cut-off' frequency which depends on material parameters. In this paper, we are concerned only with behaviour in the low frequency conduction.

As described by the Carr–Helfrich mechanism, the response of the system is controlled by the voltage, not the field. The subsequent behaviour is then described in terms of voltages.

As the voltage is increased, at some fixed frequency below the cut-off frequency, the system undergoes various transitions from straight or oblique convective rolls to less symmetrical patterns [14]. Near ten volts the system undergoes a transition from continuous convective rolls to a somewhat turbid state called dynamic scattering mode 1 (DSM 1), or primary scattering [15]. These broken-up convective rolls maintain a general orientation along the original roll axis [16]. The anisotropic nature of this state is verified through differences in the transmitted intensity of light polarized parallel and perpendicular to the original director orientation [17]. Increasing the applied voltage increases the

*Author for correspondence; e-mail: mcclymer@maine.edu

Liquid Crystals ISSN 0267-8292 print/ISSN 1366-5855 online © 2000 Taylor & Francis Ltd
http://www.tandf.co.uk/journals

break-up of the convective rolls until small roll elements are oriented randomly in space. This second, even more turbulent, state is referred to as dynamic scattering mode 2 (DSM 2), or as secondary scattering [18]. The increased symmetry of DSM 2 shows up in the similarity of the transmitted light polarized parallel and perpendicular to the original director orientation. As the DSM 2 transition is reached the system's memory of its original orientation is lost. These two scattering states are sometimes denoted as anisotropic and isotropic turbulence, respectively [17]. Even after the technological promise of these scattering states was superseded by newer technologies they continued to be of interest as an easily accessible example of turbulent–turbulent phase transitions [2, 19, 20] which include the more elusive transition in superfluid He II.

The non-equilibrium transition between the two turbulent states DSM 1 and DSM 2 was studied by ramping the applied voltage up and down at various rates (with no magnetic field) [2, 14, 21]. At non-zero ramp rates the transition is hysteretic with a claimed square root dependence on the ramping rate. This hysteresis width vanishes at zero ramp rate, indicating a supercritical transition between DSM 1 and DSM 2. It is further observed that DSM 1 is unstable with respect to nucleation of DSM 2 so that the two states do not coexist and the formation of DSM 2 from DSM 1 can be described by classical nucleation theory. In the context of equilibrium thermodynamics, as pointed out by Zimmerman [20], this result is surprising as such local transitions are connected to hysteretic transitions.

While both DSM 1 and DSM 2 appear turbulent, their underlying structure is most easily studied by turning off the electric field revealing disclination loops as responsible for the scattering nature of both these states. The disclination loops arising from DSM 1 decay much more rapidly than the denser loops visible in DSM 2 [2, 17, 20, 22].

2. Experimental

The nematic liquid crystal MBBA was sandwiched between two conducting glass slides separated by 135 μm. This large spacing was chosen as it seems to provide the most contrast in viewing structure in DSM 2. The active area of the cell was about 1 cm^2. This large size combined with the small wavelength of the distortions makes it a large aspect ratio system. The temperature of the sample was maintained at 27 ± 0.1°C. The MBBA has a conductivity of $10^{-9}\,\Omega^{-1}\,cm^{-1}$ and a cut-off frequency of approximately 300 Hz. The a.c. electric field was computer controlled, with the frequency fixed at 50 Hz, well below the cut-off frequency and high enough to avoid d.c. effects.

Figure 1 shows the configuration of the experimental set-up. The sample cell is placed between the pole faces of an electromagnetic so that the magnetic field is perpendicular to the applied electric field. The magnetic field, through the positive diamagnetic susceptibility of MBBA, tends to align the director in the plane of the sample, providing a competing interaction with the electric field, which aligns the director perpendicular to the plane of the sample through the Carr–Helfrich mechanism. The result due to this magnetic field and interactions with the rubbed glass surface (rubbed to produce planar alignment) is to give an initially planar director configuration parallel to the magnetic field. The cell is viewed along the electric field direction using a long working distance microscope and CCD camera (512×512 pixels) with a digitized output of 256 grey levels. A fiber optic bundle transports the illumination from a d.c. powered quartz-halogen lamp to the electromagnet where it passes through a polarizer so that the transmitted light is polarized parallel to the magnetic field. No analyser is used (typically). The CCD camera is connected to both a frame grabber and a VCR so that the images may be examined in real time and archived for later use.

3. Surface states

Our first observations in this system were made by placing widely separated drops of the liquid crystal between the electrodes to give four or five separate systems for study on the same slide. While most drops would immediately exhibit travelling waves (TW) upon application of the appropriate fields, we found that travelling wave states did not always form immediately in some drops. In a few instances no travelling waves would form even after several hours. The individual drops were studied and a difference was found between those that exhibited TW and those that did not. The samples exhibiting travelling waves rotated the plane of polarization of obliquely incident light whereas the drops not exhibiting TW showed no polarization rotation. We interpret this polarization rotation to be caused by a coherent surface structure.

The existence of this coherent surface structure, which we represent schematically in figure 2, may be shown by observing the sample in polarized light at some oblique angle from the surface normal [11, 12, 23]. In this way, light traversing the sample will see a twist in the director field near the surfaces due to the surface walls. The light adiabatically follows the twist so that its plane of polarization is rotated. The rotation can be measured by rotating the analyser away from its crossed position to extinguish the light. These types of bend–splay or 'Néel' walls and defects in nematics in a magnetic field

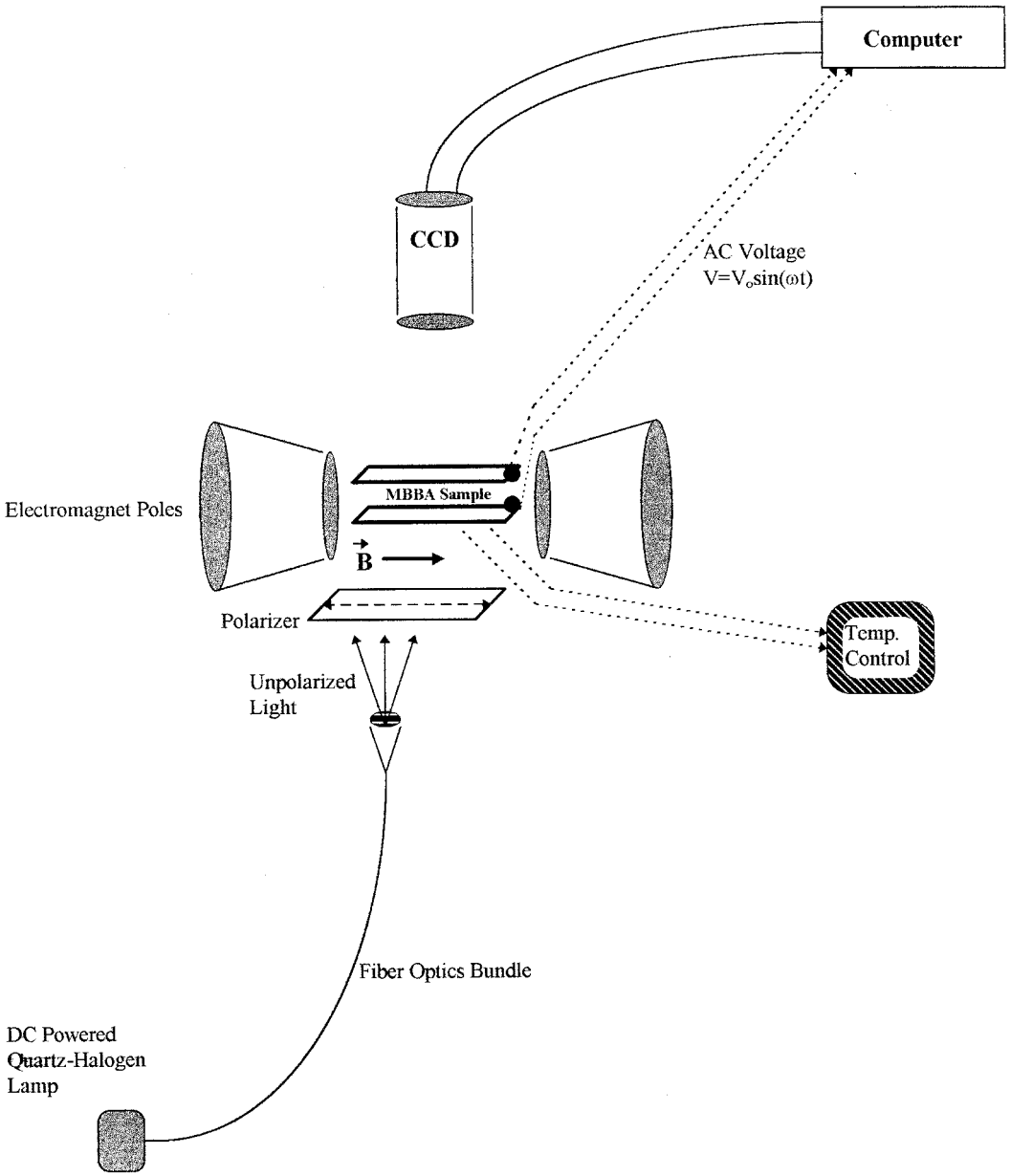

Figure 1. Experimental arrangement. An analyser is inserted in the light path for some experiments as indicated in the text.

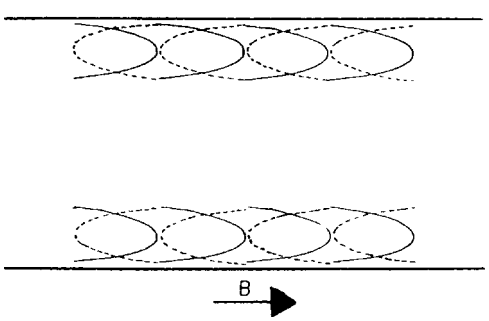

Figure 2. Orientation of the surface bend–splay walls: the solid line indicates structure in the foreground, the dashed line indicates structures in the background.

were studied by Helfrich [24] and Ranganath [25]. The bend–splay walls of opposite orientation are separated by wedge disclinations similar to Block lines in magnetism.

Figure 3 shows wedge disclinations and the effects of the bend–splay surface walls while the sample is undergoing transverse flow. The convective rolls (and the fluid) in the centre region of figure 3 (*a*) are moving to the right while the rolls in the regions above and below it (somewhat out of focus) are moving in the opposite direction. The regions are separated from each other by lines of intensive scattering that act as nucleation sites for disclination loops [22, 26]. Viewing along the surface normal between crossed polarizers, with the removal

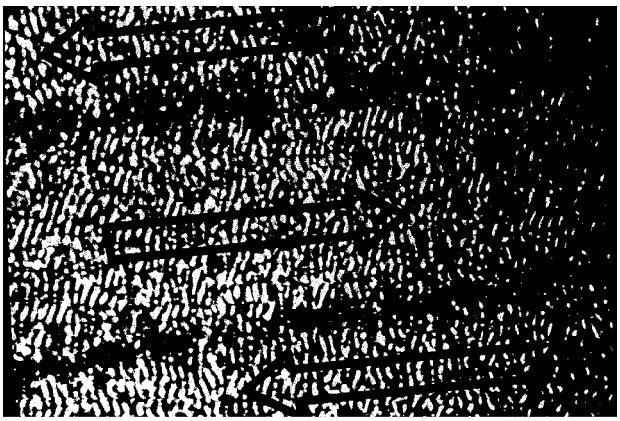

(*a*)

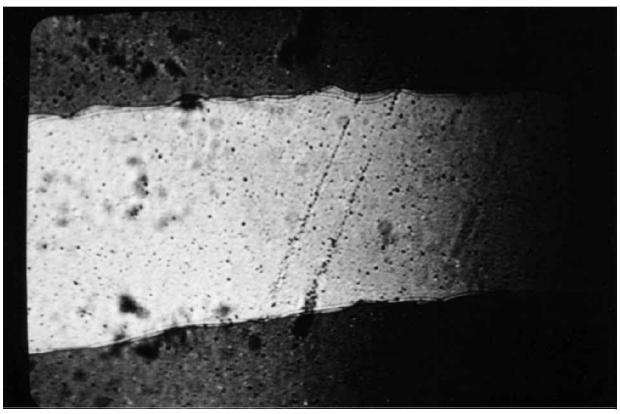

(*b*)

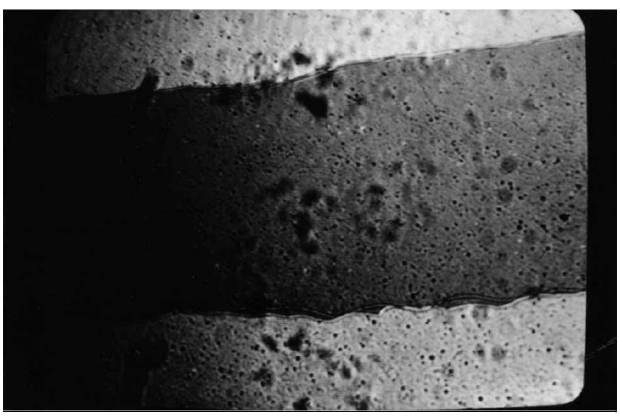

(*c*)

Figure 3. (*a*) Regions exhibiting transverse flow separated by lines of intensive scattering, which are wedge disclinations; the flow within each region is in opposite directions. (*b*) Same as in (*a*) except the electric field is turned off while retaining the magnetic field; the polarizer is parallel to the magnetic field and the analyser rotated + 10° from the crossed position. (*c*) Same as in (*b*) except the analyser is rotated − 10°.

of the electric field, shows a homogeneous sample in which the different flow regions are separated by two disclination lines, one each at the top and bottom surfaces. These are the wedge disclinations (Block lines) discussed above. Figure 3 (*b*) gives a view of the sample at an angle of 10° from the surface normal with the analyser rotated 10° (ccw) to extinguish part of the sample. When the analyser is rotated 10° in the other direction (or if the direction of observation is changed to − 10°), the light and dark regions interchange as shown in figure 3 (*c*). It is important to note that we do not observe travelling waves in the absence of this effect.

While the creation of the surface wall requires both a magnetic field and a sample undergoing electrohydrodynamic convection, once formed the surface walls last for months even with both fields removed. A similar surface state has been discussed by Dozov and Durand [27] in which they clearly describe a dynamic coupling process in which a nematic with positive dielectric anisotropy and strong planar boundary conditions at one surface, and weak homeotropic anchoring at the other surface, can undergo an anchoring-breaking transition which can give rise to a half-turn twisted structure as we describe (see figure 6 in [27]). The similarity to our system arises from the strong planar surface anchoring and the near homeotropic alignment in the bulk at the flow alignment angle as a consequence of the Carr–Helfrich effect, thus mimicking a positive dielectric anisotropy. Since we have two such planar–perpendicular interfaces our system can relax to form two such stable textures, one at each surface.

We can borrow from the work of Dozov and Durand on the dynamic coupling that leads to this stable state to estimate the extent of these walls. Consider the usual 'Carr' picture of the director orientation in which the director goes from being planar at the surface to a homeotropic orientation in the bulk of the sample. As the field is switched off the director near the surface rotates towards a planar orientation with time constant $\tau_s = \gamma\xi^2/K$, setting up a surface flow (ξ is the surface extrapolation length). This surface flow diffuses away from the surface with a time constant $\tau = \rho d^2/\eta$, (ρ is the mass density, γ and η are viscosities and K is an elastic constant). During the reorientation time the surface flow diffuses a distance given by $d^2 \approx \gamma\xi^2\eta/K\rho$. Using typical values, $d \approx 10\,\mu m$. Since our cell is much larger than this size, two surface walls are set up.

These surface states are present, as a consequence of the applied magnetic field, in all of the experiments to be described, even when the magnetic field strength is reduced to zero.

4. DSM 1 → DSM 2 transition

The DSM 1 and DSM 2 transition in the presence of the competing magnetic field is qualitatively different

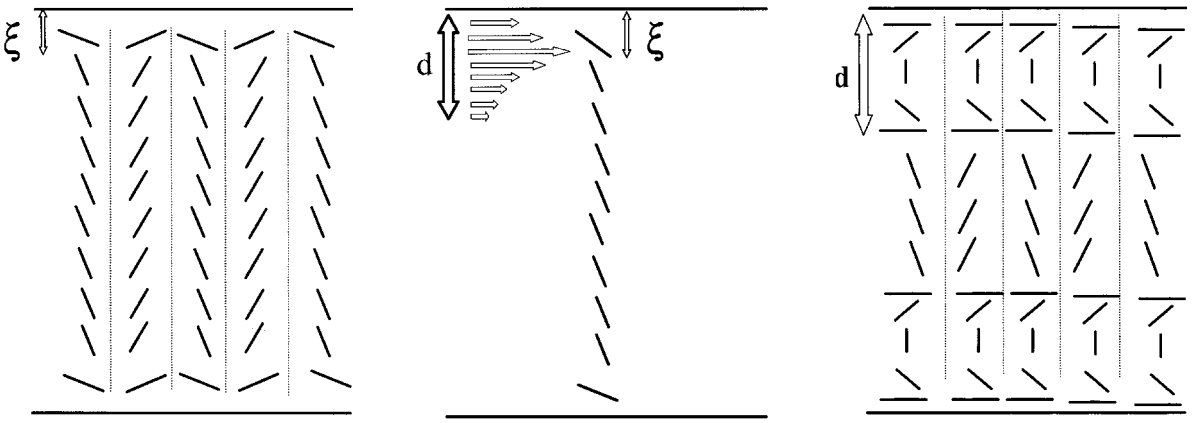

Figure 4. (*a*) Director oriented at the flow alignment angle in the bulk due to electrohydrodynamic interactions; the applied electric field is from plate to plate. The dotted lines indicate the walls separating oppositely oriented regions; the surface correlation length is indicated. (*b*) Removal of the electric field allows the surface director to reorient, setting up a flow indicated by the horizontal arrows. This flow field causes reorientation of the director as indicated. (*c*) After reorientation, stable 'pi-walls' form at both surfaces. These structures will undergo further reorientation to enter a minimum energy configuration.

from the zero field case. Instead of the system becoming more isotropic in the DSM 2 state, characterized mainly by the break-up of the convective rolls, we find the DSM 2 state retains the symmetry and wavelength of the DSM 1 state [23]. Figure 4 shows the result of a voltage jump from zero to 140 V in a 0.8 T magnetic field, which is above the DSM 1 to DSM 2 transition. The system enters a DSM 1 state from which DSM 2 nucleates and grows. The photograph in figure 5 captures the state before DSM 2 has completely filled the field of view. Both DSM 1, the lighter region, and DSM 2, the region in the centre and around the periphery, can be seen. The convective rolls are visible in both dynamic scattering modes, continuous at the spatial transition between the two scattering regimes and with the same wavelength. The only apparent difference between the two states is their relative scattering efficiencies. The scattering efficiency is due to the differing density (and lifetime) of disclination loops as discussed later in this paper and elsewhere [20, 22].

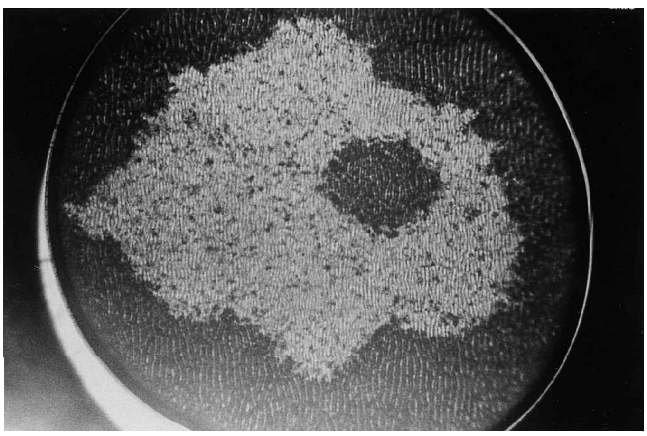

Figure 5. Transient coexistence of DSM 1 and DSM 2 (darker region) showing convective flow cells four seconds after a voltage jump from 0 to 140 V in a 0.8 T magnetic field.

Both dynamic scattering states, with the competing magnetic field, possess the same macroscopic symmetry. This continuous symmetry implies the possibility of a continuous transition between the two states. We explore the effect of the magnetic field and the surface deformation on the non-equilibrium transition between DSM 1 and DSM 2 by measuring the transmitted light intensity as the applied a.c. field is ramped up and down. The resulting curves, an example of which is shown in figure 6, show a hysteresis as a function of ramp rate and magnetic field strength. Plotting this gap (ΔV) as a function of magnetic field at a fixed ramp rate, figure 7, shows a linear relation described by $\Delta V = -2.55\mathbf{H} + 60.8$ where V is measured in volts and $\mathbf{H}$ in kG. Extrapolating this linear behaviour to where the hysteresis gap vanishes, we find a critical field, $\mathbf{H}_0 = 23.8$ kG, which is well above our experimentally accessible field of 10 kG.

We use this critical magnetic field strength to define a dimensionless magnetic field $h = (\mathbf{H}_0 - \mathbf{H})/\mathbf{H}_0$. The hysteresis data is well described by the equation

$$(\Delta V)^{-1} = A_1 h^{\alpha} r^{\beta} + \frac{A_2}{h} \qquad (1)$$

which has the form of a power law and a field-dependent background. In this equation A_1 and A_2 are constants, r is the ramp rate in volts per second and the exponents

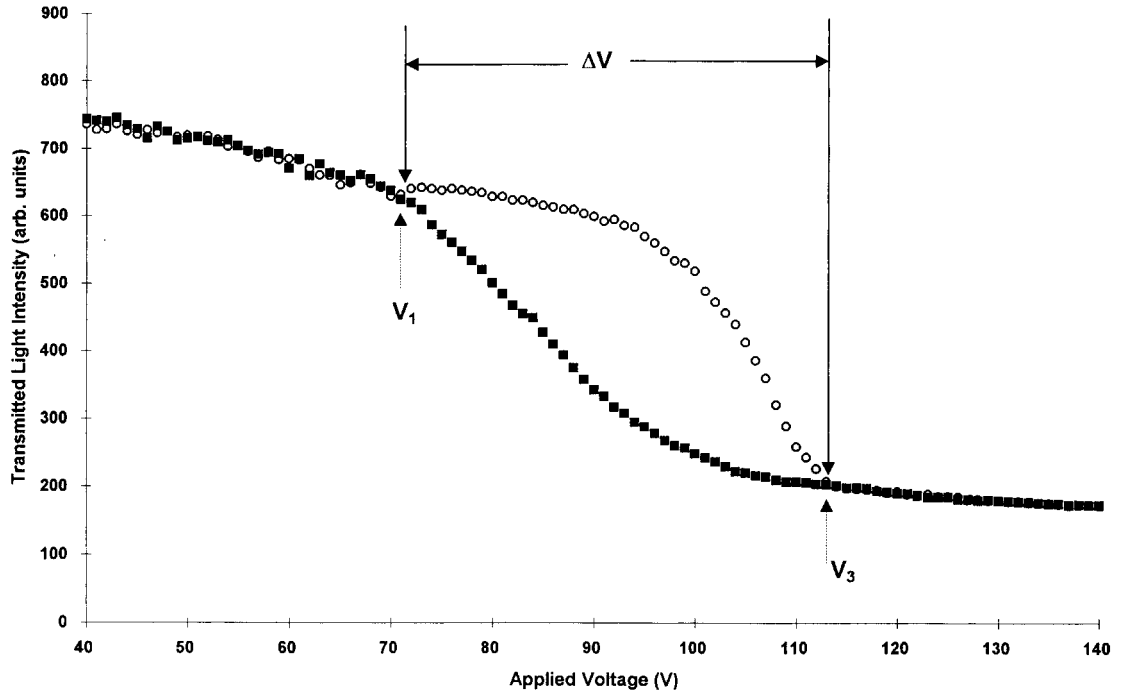

Figure 6. Hysteresis in the transmitted light intensity near the DSM 1↔DSM 2 transition in a 0.4 T magnetic field at a ramp rate of 78.2 mV s^{-1}. Open circles represent ramping the voltage up while filled squares represent ramping the voltage down.

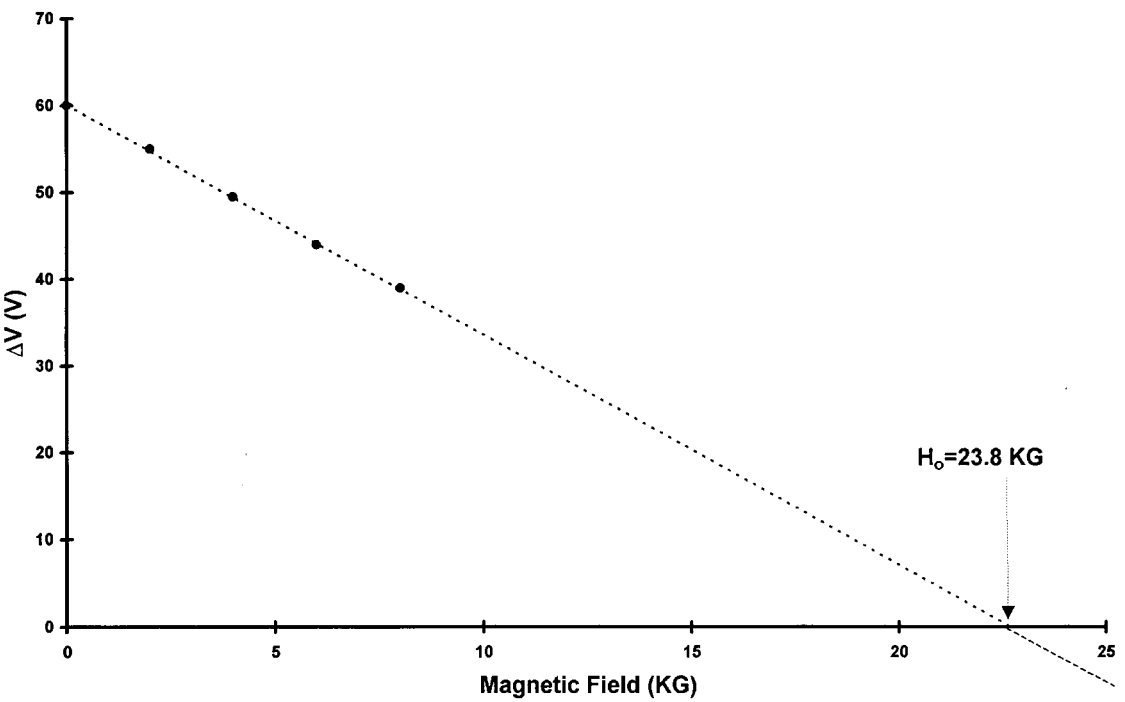

Figure 7. Hysteresis gap dependence on the magnetic field at a fixed ramp-rate of 496.7 mV s^{-1}.

are $\alpha = -0.4$ and $\beta = -1.3$ (figure 8). This result is quite different from the value of 0.5 reported for the zero field case [2, 21]. We do not believe this experimental discrepancy important as the earlier result had only a few data points at small r where the curvature is important. Additionally, the data were only shown to be consistent with a model curve, no fitting of the parameters was done.

The data collapse to a single curve when the scaling parameter $\Delta V/h^{\gamma}$ is plotted against r/h^{δ} with $\gamma = -0.01$

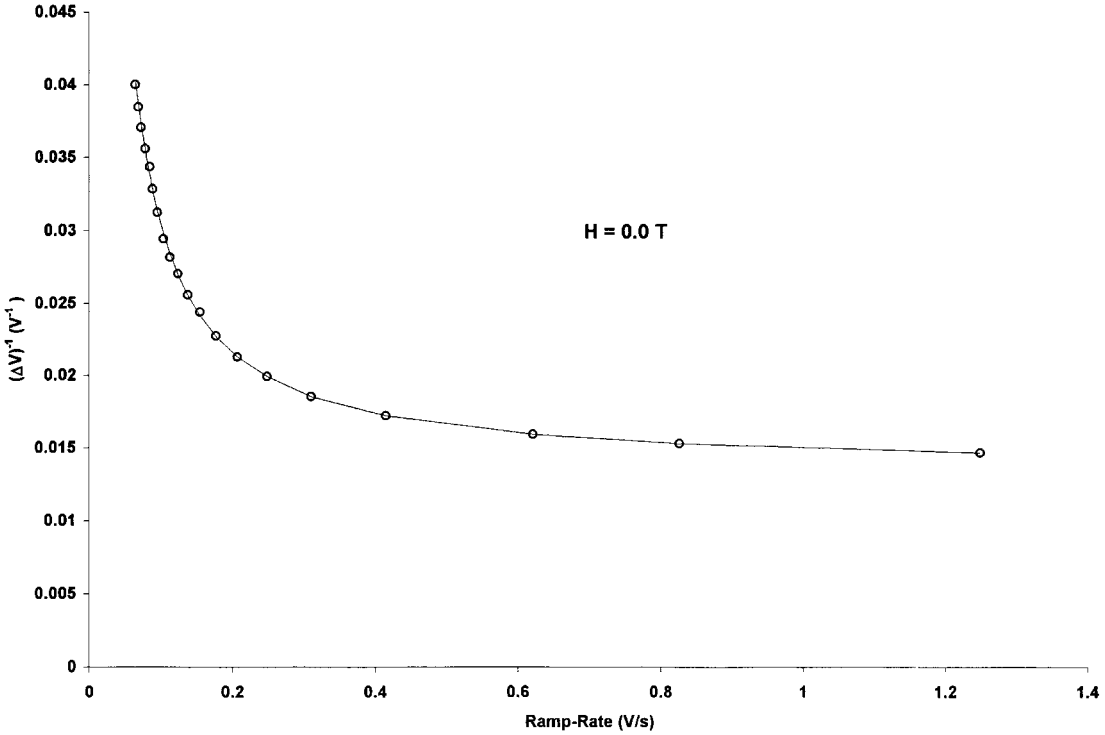

(*a*)

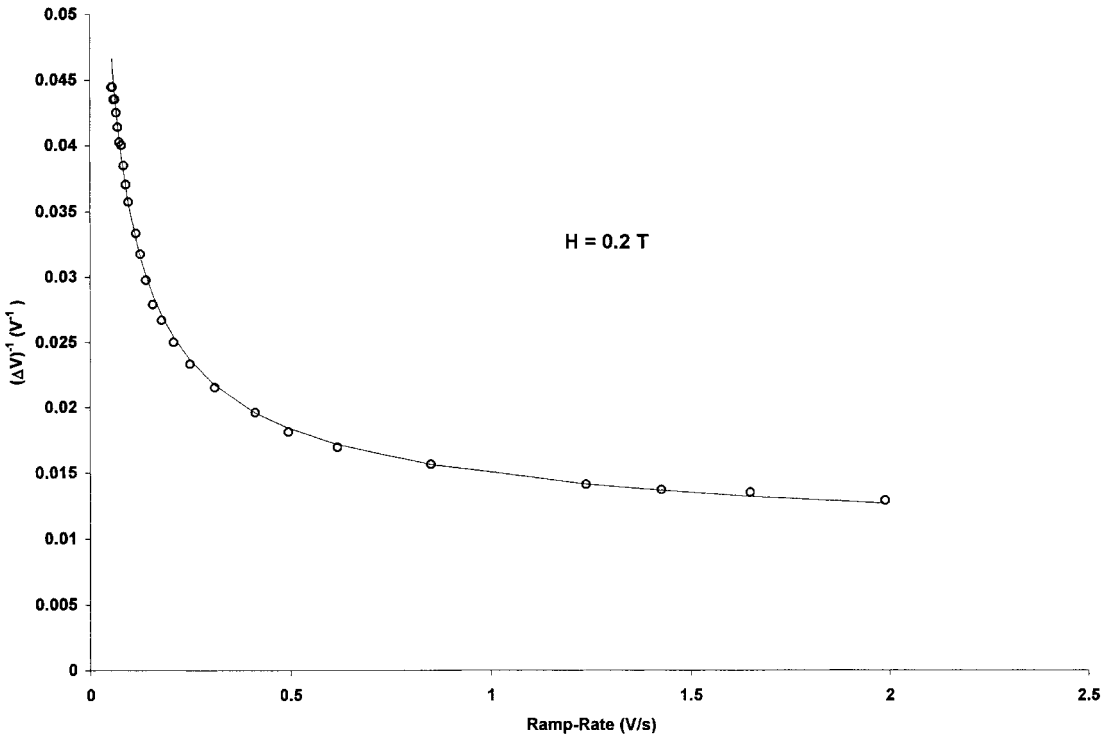

(*b*)

Figure 8. Power law fits of the inverse hysteresis gap width vs. rap rates at various magnetic field strengths: **H** = (*a*) 0.0, (*b*) 0.2, (*c*) 0.4, (*d*) 0.6, (*e*) 0.8 T. Open circles are the experimentally measured inverse hysteresis gap widths while the solid curves are power law fits using equation (1).

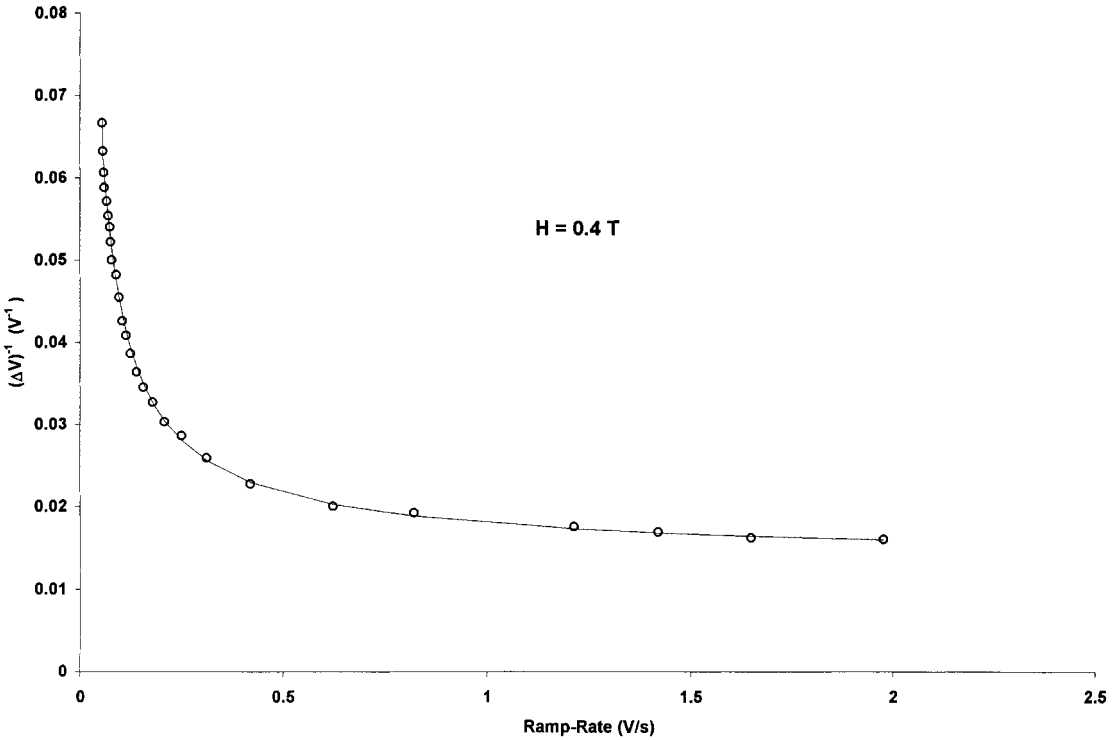

(*c*)

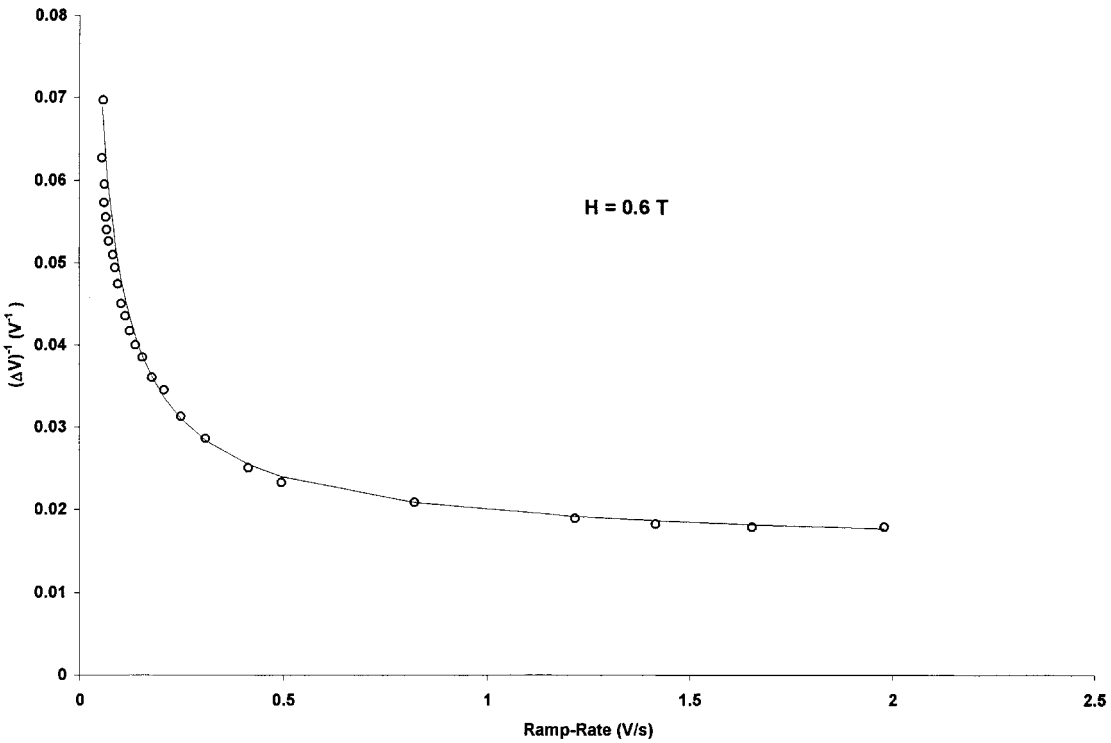

(*d*)

Figure 8. (*continued*).

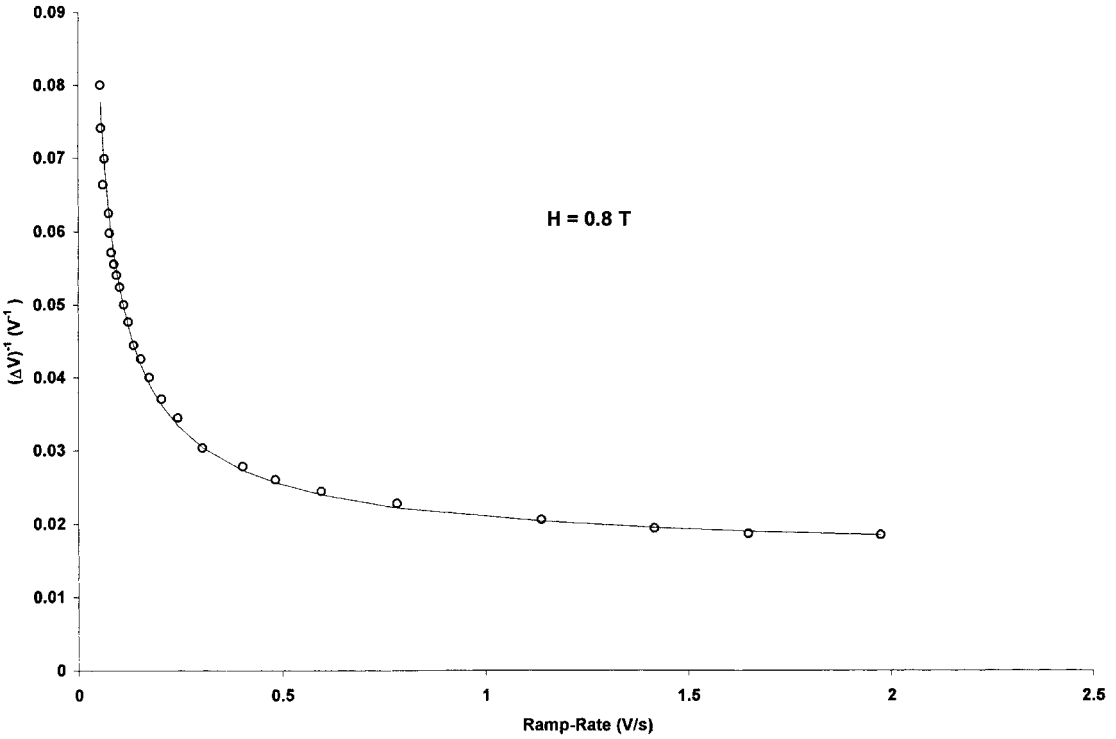

(*e*)

Figure 8. (*continued*).

and $\delta = -3.3$. As figure 9 shows, this scaling is fairly successful for small ramp rates but fails to describe the background at large ramp rates well.

5. Coexistence of DSM 1 and DSM 2

A surprising finding is the formation of a coexisting DSM 1 and DSM 2 state we refer to as DSM 1&2. Earlier work shows that DSM 2 nucleates [17, 18] out of DSM 1 and that both states may coexist only in a transient state [28].

We first find evidence for this mixed state at our highest magnetic field strength, 0.8 T. As the data show, the large magnetic field causes the voltage ranges for the various states to increase. We observe the mixed state between 80 and 90 V. The width of the coexistence region decreases with decreasing magnetic field, with coexistence persisting down to zero field. One reason this mixed state is observed is that we are studying the system at very low magnification, giving a large observation area. Observation of a subregion would typically not show both phases except over a very narrow voltage range.

The signature of the mixed state, on increasing voltage, is the formation of a dark DSM 2 region in a DSM 1 sea. The DSM 2 region moves about the observed area in a random walk-like way. Repeated cycling of the voltage shows that the DSM 2 forms in different parts of the sample. This mobility and lack of a site-specific nucleation indicate that the DSM 2 is not forming because of defects or inhomogeneities in the sample cell itself. When the voltage is first increased, DSM 2 first forms and grows to a characteristic size in only a few minutes. The growth stops and the characteristic size remains the same, as the DSM 2 region migrates about the sample. Observations over an hour show no further change in the state. As the voltage increases, DSM 2 becomes the dominant state; the minority DSM 1 is also not pinned to a specific site in the sample although all of the DSM 1 does group together.

6. Surface walls and DSM 1 → DSM 2 transition

Why are the two scattering modes different? What actually changes at the transition? Our previous results, and those of others, show that DSM 2 consists of a dense grouping (we see no evidence of entangled loops) of long lived disclination loops, as compared with the lower density and quickly decaying disclination loops associated with DSM 1. We think part of the answer to the above questions can be found by studying the transition and orientation of the surface state at the same time.

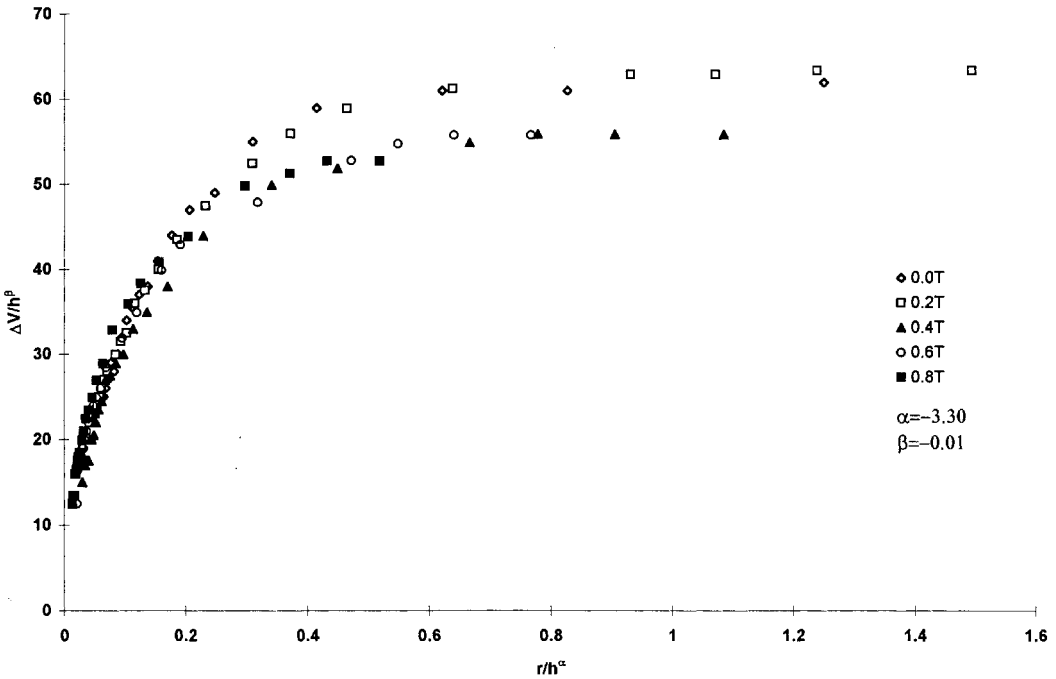

Figure 9. Scaled hysteresis gap width vs. scaled ramp rate for 0.0 T (filled circles), 0.2 T (empty squares), 0.4 T (filled triangles), 0.6 T (empty rhombus) and 0.8 T (filled squares).

We do this experimentally by viewing a large area at low resolution so that the individual convective rolls (as in figure 4) can no longer be seen. In this way many more regions of DSM 1 and DSM 2 can be seen. We apply a voltage above the DSM 1 and DSM 2 transition and photograph DSM 2 nucleating out of DSM 1. The electric field is then turned off and the associated disclination field viewed using obliquely incident light and rotated analysers to capture information on the alignment of the surface walls.

Figure 10 shows the results of this procedure. The dark DSM 2 regions and the lighter DSM 1 regions are visible in 10 (*a*). Removal of the electric field and rotation of the analyser extinguishes part of the sample as shown in 10 (*b*). The region that originally showed only DSM 1 shows a uniform colour indicating a homogeneous alignment of the surface walls. In contrast, the region that exhibited DSM 2 consists of patches of bright and dark regions indicating that the surface walls reverse at the boundary through wedge defects, the match-up is not perfect as the system continued to evolve between the photographs (a few seconds). These time-varying irregular patches show that the orientation of the surface walls on the two surfaces are dynamic. When the sample is not dark between crossed polarizers the surface walls are oriented in the same sense, either parallel or anti-parallel to the magnetic field. When the sample does appear dark the walls are oriented in the opposite sense (the wall on the top surface pointing in the opposite direction from the wall on the bottom surface). The DSM 2 state has a much more irregular pattern of surface states compared with the uniform orientation that corresponds to DSM 1. These results show that the surface structure and defect density are related. The question then is how are they related and does one cause the other?

As we argue elsewhere [18, 23], when the surface walls have the same orientation not only do we see rotation of obliquely incident light, the interaction between the convective flow and surface walls results in a net force responsible for the travelling waves. If the orientation on both surfaces is reversed the force is in the opposite direction and flow is established in this direction. As shown in figures 2 and 3 (*a*), the boundary between these two orientation states is separated by a disclination line (one at each surface) and the shear flow nucleates disclination loops which are responsible for the enhanced scattering. If the walls on the two surfaces are of the opposite sense there is no net force and no rotation of the light.

We can use this idea to postulate a relation between the scattering state and the surface walls. Within the DSM 1 region there is uniform alignment of the surface walls resulting in no relative flow. At the DSM 1 and DSM 2 boundary the surface walls are of opposite orientation—see the lines of intensive scattering in

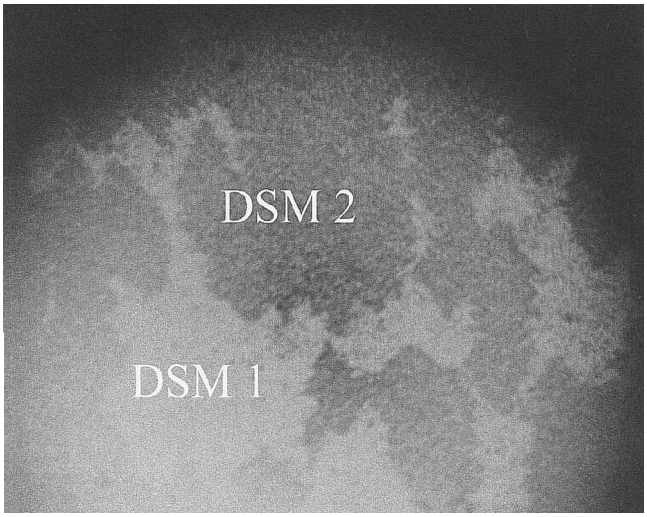

(*a*)

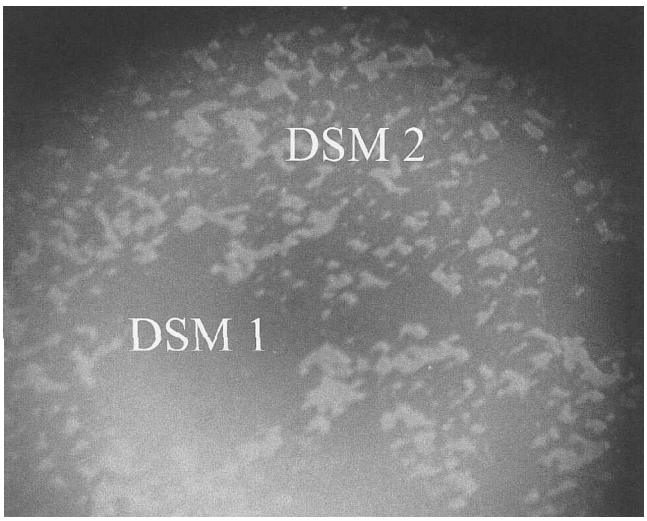

(*b*)

Figure 10. (*a*) Shows DSM 2 nucleating out of DSM 1 after a voltage jump above the DSM 1 → 2 transition voltage. Before the darker DSM 2 can fully cover the region the electric field is turned off revealing (*b*) the orientation of the surface walls as indicated in the text.

figure 3 (*a*)—and shear flow nucleates disclination loops. Within DSM 2, the region of uniform surface walls has a much smaller characteristic size and, since the system is far from equilibrium, these regions wander around the top and bottom surface independently. When the top and bottom surface states have the same orientation, flow is induced in one direction while in an adjacent region the orientation may be in the opposite sense, so flow is induced in that alternate direction resulting in strong local shear and enhanced nucleation of disclination loops. As these surface walls migrate around the surface the bulk is randomly subjected to strong local shearing motion [26] which nucleates disclination loops that are transported by the convective flow. It is these disclination loops which are responsible for the strong scattering observed in DSM 2 [2, 15, 18]. For this system then, it is the randomizing of surface orientation that leads to local shear flow that enhances nucleation of disclination loops, giving DSM 2 its enhanced scattering.

Can this mechanism also be in play to describe the DSM transitions when there are no surface walls, in samples never exposed to magnetic fields? The answer is yes, as the cause of the transition between the two states is shear-induced disclination loops. The formation of these loops is certainly abetted by the shearing motion of the migrating surface walls as outlined above. In the no-surface-wall case another cause of the shear needs to be found. A possible mechanism causing the sheer is the anisotropic to isotropic transition in which the convective rolls break up [17]. These more randomly distributed, and smaller, convective rolls nucleate the disclination loops which are the hallmark of DSM 2.

7. Summary

We have determined the existence of a metastable surface state caused by interaction between convecting nematic liquid crystal and a magnetic field. This surface distortion is in some way responsible for the travelling waves we observe over wide frequency and voltage ranges. A phenomenological picture of convective roll cells interacting with the surface state leading to transverse forces has been developed. It is suggested that the transverse forces are responsible for the nucleation of disclination loops. The formation of DSM 2 and DSM 1 is a result of the formation of Ranganath bend–splay defects and an increase in local shear. Since the surface walls are not present if no magnetic field is applied, this mechanism is not applicable to the zero field DSM 2 transition, although increased shear due to the breakup of the DSM 1 convective rolls may be responsible for the increased turbidity of DSM 2.

The magnetic field stabilizes the DSM 1 and DSM 2 transition, preventing DSM 2 from becoming turbulent. The DSM 2 state is seen to possess the same symmetry as DSM 1 and to differ only in production and rate of decay of disclination loops. The transition between these two states is well described by a scaling relation put forward in this paper.

A magnetic field-dependent coexisting DSM 1&2 state has been observed for the first time. Coexisting phases are consistent with the type of nucleation observed but inconsistent with the lack of hysteresis observed by ourselves and others.

References

[1] See for instance De Gennes, P. G., and Prost, J., 1993, *The Physics of Liquid Crystals*, 2nd Edn (Oxford: Clarendon Press); Chandrasekhar, S., 1992, *Liquid Crystals*, 2nd Edn (Cambridge: Cambridge University Press).

[2] Kai, S., and Zimmermann, W., 1989, *Prog. theor. Phys. Suppl.*, **99,** 458.

[3] Kozlowski, R. W. H., and Carr, E. F., 1984, *Mol. Cryst. liq. Cryst.*, **111,** 161; Kozlowski, R. W. H., and Carr, E. F., 1981, *Mol. Cryst. liq. Cryst.*, **64,** 299; Carr, E. F., 1978, *Liquid Crystal and Ordered Fluids III*, edited by J. F. Johnson and R. S. Porter (Plenum Press), p. 165.

[4] Orsay Liquid Crystal Group, 1971, *Mol. Cryst. liq. Cryst.*, **12,** 251.

[5] Bodenschatz, E., Zimmermann, W., and Kramer, L., 1988, *J. de Physique*, **49,** 1875.

[6] Kai, S., Chizumi, N., and Kohno, M., 1989, *Phys. Rev.*, **40,** 6554.

[7] Joets, A., and Tibotta, R., 1988, in *Propagation in Systems Far from Equilibrium*, edited by J. E. Wesfreid, H. R. Brand, P. Manneville, G. Albinet and N. Boccara (Berlin: Springer-Verlag); Joets, A., and Tibotta, R., *Phys. Rev. Lett.*, **60,** 2164.

[8] Rehberg, I., Rasenat, S., and Steinberg, V., 1989, *Phys. Rev. Lett.*, **62,** 756; Rehberg, I., Rasenat, S., de la Torre Juares, M., Schopf, W., Horner, F., Ahlers, G., and Brand, H., 1991, *Phys. Rev. Lett.*, **67,** 596.

[9] Dennin, M., Treiber, M., Kramer, L., Ahlers, G., and Cannell, D., 1996, *Phys. Rev. Lett.*, **76,** 319; Dennin, M., Cannell, D., and Ahlers, G., 1995, *Mol. Cryst. liq. Cryst.*, **261,** 377.

[10] Treiber, M., Eber, N., Buka, A., and Kramer, L., 1997, *J. Phys. II*, **7,** 649.

[11] Carr, E. F., and McClymer, J. P., 1990, *Mol. Cryst. liq. Cryst.*, **182B,** 245.

[12] McClymer, J. P., 1991, *Mol. Cryst. liq. Cryst.*, **199,** 233.

[13] Williams, R., 1963, *J. chem. Phys.*, **39,** 384.

[14] Joets, A., and Ribotta, R., 1984, in *Cellular Structures in Instabilities*, edited by J. E. Wesfried and S. Zaleski (Berlin: Springer-Verlag).

[15] Heilmeier, G. H., Zanoni, L. A., and Barton, L., 1968, *Proc. IEEE*, **56,** 1162; Kapustin, A. P., and Vistin, L. K., 1965, *Kristallografiya*, **10,** 118; Elliot, G., and Gibson, J. G., 1961, *Nature*, **205,** 995.

[16] Joets, A., and Ribbota, R., 1986, *J. de Physique*, **47,** 595.

[17] Yamazaki, H., Kai, S., and Hirakawa, K., 1985, *Mol. Cryst. liq. Cryst.*, **122,** 41.

[18] Sussmann, A., 1972, *Appl. Phys. Lett.*, **21,** 269.

[19] Kai, S., Zimmermann, W., Andoh, M., and Chizumi, N., 1990, *Phys. Rev. Lett.*, **64,** 1111.

[20] Zimmermann, W., 1991, *MRS Bull.*, **16,** 46.

[21] Kai, S., Zimmermann, W., Andoh, M., and Chizumi, N., 1989, *J. phys. Soc. Jpn.*, **58,** 3449; Kai, S., Zimmermann, W., and Andoh, M., 1990, *Mod. Phys. Lett. B*, **4,** 767.

[22] Shehadeh, H. M., and McClymer, J. P., 1997, *Phys. Rev. Lett.*, **79,** 4207.

[23] McClymer, J. P., Carr, E. F., and Shehadeh, H., 1994, *Spatio-Temporal Patterns*, edited by P. E. Cladis and P. Palffy-Muhoray, SFI Studies in the Science of Complexity, Proc. Vol. XXI (Addison-Wesley), p. 367.

[24] Helfrich, W., 1968, *Phys. Rev. Lett.*, **21,** 1518.

[25] Ranganath, G. S., 1988, *Mol. Cryst. liq. Cryst.*, **154,** 43.

[26] De Gennes, P. G., 1976, in *Molecular Fluids*, edited by Balian Weill (Gordon and Breach), pp. 375–400; de Gennes, P. G., 1974, *J. de Phys. Lett.*, **35L,** 271.

[27] Dozov, I., and Durand, G., 1998, *Liq. Cryst. today*, **8,** 1.

[28] Kai, S., Andoh, M., and Yamaguchi, S., 1992, *Phys. Rev. A*, **46,** R7375.